Design Analysis of Staggered InGaN Quantum Wells Light-Emitting Diodes at 500–540 nm

Hongping Zhao, Ronald A. Arif, and Nelson Tansu, *Member, IEEE*

***Abstract*—Staggered InGaN quantum wells (QWs) are analyzed as improved active region for light-emitting diodes (LEDs) emitting at 500 nm and 540 nm, respectively. The calculation of band structure is based on a self-consistent 6-band $k{\cdot}p$ formalism taking into account the valence band mixing, strain effect, and spontaneous and piezoelectric polarizations as well as the carrier screening effect. Both two-layer staggered $In_xGa_{1-x}N/In_yGa_{1-y}N$ QW and three-layer staggered $In_yGa_{1-y}N/In_xGa_{1-x}N/In_yGa_{1-y}N$ QW structures are investigated as active region to enhance the spontaneous emission radiative recombination rate (R_{sp}) for LEDs emitting at 500 nm and 540 nm. Analysis of the spontaneous emission radiative recombination rate (R_{sp}) shows significant enhancement for both two-layer staggered InGaN QW and three-layer staggered InGaN QW, in comparison to that of the conventional $In_zGa_{1-z}N$ QW. The studies of the carrier lifetime indicate a significant reduction of the carrier lifetime for staggered InGaN QWs, which contribute to the enhancement of the radiative efficiency for both two-layer staggered InGaN QW and three-layer staggered InGaN QW LEDs emitting at 500 nm and 540 nm.**

***Index Terms*—III-Nitride, diode lasers, InGaN QWs, light-emitting diodes, radiative efficiency, staggered InGaN QWs.**

I. Introduction

The InGaN-based quantum wells (QWs) attract a lot of interest due to their use as the active region in visible and near UV III-Nitride light-emitting diodes (LEDs) and laser diodes [1]–[5]. However, there are major challenges for high-efficiency III-Nitride LEDs based on conventional InGaN QWs, as follow: 1) high threading dislocation densities due to the lack of lattice-matched substrate and phase separation in high-In-content InGaN QWs; 2) the existence of the built-in electrostatic fields in InGaN QWs due to the existence of polarization fields in QW. The InGaN QWs grown on GaN template on c-plane sapphire substrate suffer from both spontaneous and piezoelectric polarization fields, which leads to charge separation effect. The spontaneous polarization (P_{spon}) field in III-Nitride materials arises from the nonideal internal cell parameters (c/a) of the wurtzite III-N [0001]-oriented materials. The piezoelectric polarization (P_{piezo}) in InGaN-based QW arises due to the lattice mismatch between the QW and barrier. The existence of the internal electric field pulls the electrons and holes to the opposite sides causing charge separation effect, which significantly reduces the electron–hole wave function overlap (Γ_{e_hh}). The significantly reduced electron–hole wave function overlap (Γ_{e_hh}) in InGaN QW leads to significant reduction in its radiative recombination rate ($\sim|\Gamma_{e\_hh}|^2$).

As the emission wavelength in InGaN QW is extended to green spectral regime and beyond, the issues mentioned earlier become more challenging. The charge separation becomes more severe, in particular for two schemes to extend the emission wavelengths into green regime ($\lambda \sim 525$ nm) or beyond as follow: 1) by increasing the In content in InGaN QW; 2) by increasing the thickness of InGaN QW. Both approaches lead to severe reduction in the electron–hole wave function overlap Γ_{e_hh} in particular for InGaN QW emitting in the green spectral regime.

Recently, several approaches have been proposed to enhance the electron–hole wave function overlap (Γ_{e_hh}) such as 1) the use of nonpolar InGaN QW [6], 2) the use of InGaN QW with δ-AlGaN layer [7], [8], 3) staggered InGaN QW [9], [10], 4) type-II InGaN-GaNAs QW [11], [12] and 5) strain-compensated InGaN-AlGaN QW [13], [14]. All the recently proposed schemes focused on increasing the radiative recombination rate of the InGaN-based QW by improving the electron–hole wave function overlap in the QW.

Previously, the two-layer staggered InGaN QW employing step-function like In content in the QW had been implemented into LED device structure for emission in the blue spectral regime [9], [10]. The use of two-layer staggered InGaN QW LEDs led to improvement in output power and efficiency of the devices.

In this paper, we present comprehensive optimization studies of the staggered InGaN QW by engineering the In content and thickness of the sublayers of the staggered InGaN QWs, designed for peak emission wavelengths at 500 nm and 540 nm. In this study, both two-layer staggered $In_xGa_{1-x}N/In_yGa_{1-y}N$ QW structure and three-layer staggered $In_yGa_{1-y}N/In_xGa_{1-x}N/In_yGa_{1-y}N$ QW structure are investigated to optimize both the electron–hole wave function overlap (Γ_{e_hh}) and spontaneous emission radiative recombination rate (R_{sp}) for LEDs emitting at 500 nm and 540 nm. For the QWs emitting with peak emission wavelength $\lambda_{peak} = 500$ nm, the characteristics of the optimized two-layer staggered $In_{0.3}Ga_{0.7}N$ ($d_{w1} =$ 1.8 nm)/$In_{0.14}Ga_{0.86}N$ ($d_{w2} = 1.2$ nm) QW, and three-layer staggered $In_{0.14}Ga_{0.86}N$ ($d_{w1} = 0.6$ nm)/$In_{0.3}Ga_{0.7}N$ ($d_{w2} =$ 1.8 nm)/$In_{0.14}Ga_{0.86}N$ ($d_{w3} = 0.6$ nm) QW structures are analyzed and compared with those of the conventional $In_{0.25}Ga_{0.75}N$ ($d_{QW} = 3$ nm). For the QWs emitting with peak emission wavelength $\lambda_{peak} = 540$ nm, both the two-layer

Manuscript received December 16, 2008; revised February 8, 2009. First published June 23, 2009; current version published August 5, 2009. This work was supported in part by the National Science Foundation (NSF)-ECCS Award #0701421, in part by US Department of Energy (NETL program), and in part by Peter C. Rossin Assistant Professorship Funds.

The authors are with the Department of Electrical and Computer Engineering, Center for Optical Technologies, Lehigh University, Bethlehem, PA 18015 USA (e-mail: hoz207@lehigh.edu; raa4@lehigh.edu; tansu@lehigh.edu).

Color versions of one or more of the figures in this paper are available online at http://ieeexplore.ieee.org.

Digital Object Identifier 10.1109/JSTQE.2009.2016576

staggered $In_{0.32}Ga_{0.68}N$ ($d_{w1} = 2.1$ nm)/$In_{0.16}Ga_{0.84}N$ ($d_{w2} = 1.4$ nm) QW and three-layer staggered $In_{0.16}Ga_{0.84}N$ ($d_{w1} = 0.7$ nm)/$In_{0.32}Ga_{0.68}N$ ($d_{w2} = 2.1$ nm)/$In_{0.16}Ga_{0.84}N$ ($d_{w3} = 0.7$ nm) QW structures are compared to the conventional $In_{0.27}Ga_{0.73}N$ QW ($d_{QW} = 3.5$ nm).

The band structures and wave functions are obtained by utilizing a self-consistent 6-band $k{\cdot}p$ model. To take into consideration of the carrier screening effect, the Schrödinger equations and Poisson equations are solved self-consistently till the eigen energies converge. The discussion on the numerical methods utilized in these studies is described in Section III, and the details of the formalism for the self-consistent 6-band $k{\cdot}p$ for InGaN-based QW active regions are presented in [14].

The paper is organized as follows: Section II introduces the concept of two-layer staggered $In_xGa_{1-x}N/In_yGa_{1-y}N$ QW and three-layer staggered $In_yGa_{1-y}N/In_xGa_{1-x}N/In_yGa_{1-y}N$ QW structures. In Section III, the theoretical and numerical formulation is presented briefly. The spontaneous emission radiative recombination rate (R_{sp}) is discussed for staggered InGaN QWs at the emission wavelength of 500 nm and 540 nm in Sections IV and V, respectively. The carrier radiative lifetime and radiative efficiency of staggered InGaN QWs LEDs will be discussed in Section VI, and the results will be compared with those of conventional InGaN QW LEDs. The effect of the Auger recombination process on the radiative efficiency of staggered InGaN QW will be discussed in Section VII.

II. Concepts of Staggered InGaN QWs

The existence of strong electrostatic fields in the InGaN QW leads to strong energy band bending for both conduction band and valence band in the QW, which result in the spatial separation of the electrons and holes and reduce the electron–hole wave function overlap (Γ_{e_hh}). The purpose of using the staggered InGaN QW design is to enhance the electron–hole wave function overlap (Γ_{e_hh}) by engineering the band lineups of the InGaN QW, hence leading to increase in the spontaneous emission radiative recombination rate (R_{sp}) of the QW in particular for LEDs application. The concept of staggered InGaN QW studied here can be implemented as active regions in typical nitride-based LED device structures [1]–[3], [9], [10].

Fig. 1 shows the schematics of (a) the conventional $In_zGa_{1-z}N$ QW; (b) the two-layer staggered $In_xGa_{1-x}N/In_yGa_{1-y}N$ QW, and (c) the three-layer staggered $In_yGa_{1-y}N/In_xGa_{1-x}N/In_yGa_{1-y}N$ QW structures, which are surrounded by the GaN barriers. Note that the three structures have the same total QW thickness (d_{QW}). As shown in Fig. 1, the conventional $In_zGa_{1-z}N$ QW contains the uniform In content of z with the QW thickness of d_{QW}, while the two-layer staggered $In_xGa_{1-x}N/In_yGa_{1-y}N$ QW characterizes as a step-function like In content: higher In-content of x with thickness of d_{w1}, and lower In-content of y with thickness of d_{w2} ($d_{w1} + d_{w2} = d_{QW}$). In contrast to the two-layer staggered InGaN QW, the three-layer staggered $In_yGa_{1-y}N/In_xGa_{1-x}N/In_yGa_{1-y}N$ QW contains the higher In-content (x) sublayer in the center, which is sandwiched between two InGaN sublayers with lower In-content of y. The total thickness of the three-layer staggered InGaN QW is also designed as equal to $d_{QW} = d_{w1} + d_{w2} + d_{w3}$. To compare the performance of the active regions of these three structures for LED application, the In contents for the conventional InGaN QW, two-layer staggered $In_xGa_{1-x}N/In_yGa_{1-y}N$ QW and three-layer staggered $In_yGa_{1-y}N/In_xGa_{1-x}N/In_yGa_{1-y}N$ QW are designed such that all three QWs emitting at similar peak emission wavelength.

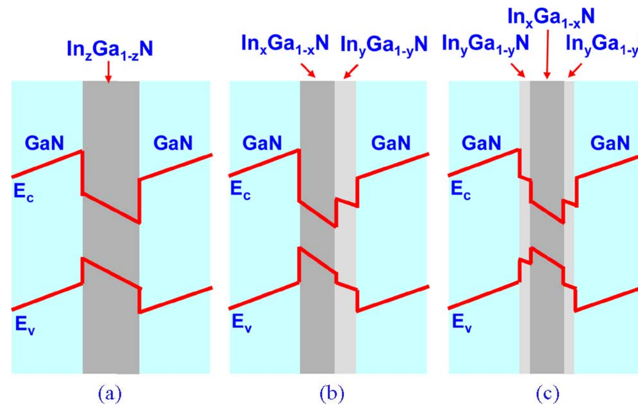

Fig. 1. Schematics of the (a) conventional $In_zGa_{1-z}N$-GaN QW, (b) two-layer staggered $In_xGa_{1-x}N/In_yGa_{1-y}N$ QW, and (c) three-layer staggered $In_yGa_{1-y}N/In_xGa_{1-x}N/In_yGa_{1-y}N$ QW structures.

Note that for three-layer staggered design, the indium compositions of the first and third layers can be in general designed with different contents. However, in our current studies, the indium contents in the first and third InGaN layers are assumed as identical and lower than that of the center region. This assumption simplifies the discussion, without losing the generality of the design.

Based on Fermi's Golden Rule, the interband transition rate is proportional to the square of their electron–hole wave function overlap Γ_{e_hh}. By engineering the energy band lineups, the electron–hole wave function overlap (Γ_{e_hh}) of the staggered InGaN QW can be significantly enhanced. Thus, the staggered InGaN QWs are expected to have higher spontaneous emission recombination rate (R_{sp}) than that of the conventional InGaN QW.

III. Theoretical and Numerical Formulation

The band structure calculation for the conventional and staggered InGaN QWs is based on self-consistent 6-band $k{\cdot}p$ formalism for wurtzite semiconductors [14]–[16]. The calculation takes into account the strain effect, the valence band mixing, and the spontaneous and piezoelectric polarizations as well as the carrier screening effect. The carrier screening effect is calculated self-consistently via the Schrödinger and Poisson equations [14], [17]. Note that the coupling between the conduction band and valence band is negligible for the case of the wide bandgap InGaN material system [15], [16], which is not taken into account in the 6-band $k{\cdot}p$ method.

To take into account the effect of the charge distribution, the confined energies and corresponding wave functions are obtained by calculating the Schrodinger's and Poisson's equations iteratively till the eigen-energy converges. For the QW structures, the momentum matrix elements ($|M_{\mathrm{sp}}|^2$) become polarization dependent including TE polarization ($M_{\mathrm{TE}}|^2$) and TM polarization ($|M_{\mathrm{TM}}|^2$). In this study, the spontaneous emission rate is obtained by averaging of the momentum matrix elements of three polarizations as $|M_{\mathrm{sp}}|^2 = (2|M_{\mathrm{TE}}|^2 + |M_{\mathrm{TM}}|^2)/3$. The details of the self-consistent numerical formulation for InGaN-based QW active regions employing 6-band $k{\cdot}p$ formalism are presented in [14].

The material parameters of binary InN, GaN for the band structure calculation are obtained from [18] and [19], which are summarized in the table in [14]. The parameters for the ternary alloy InGaN are obtained by linear interpolation of that of the binary InN and GaN, except for the energy gap of InGaN. The bandgap for $In_xGa_{1-x}N$ is obtained as follow: $E_g(In_xGa_{1-x}N) = x \cdot E_g(InN) + (1 - x) \cdot E_g(GaN) - bx(1-x)$, where the bowing parameter b is 1.4 eV [19]. The band offset ratio ($\Delta E_c{:}\Delta E_v$) of InGaN/GaN is assumed to be 0.7:0.3 [20].

The finite difference approach is employed to solve the Schrodinger's and Poisson's equations for semiconductor heterostructure/nanostructure [13], [21]. The discretisized step size is 1 Å. The thickness of the GaN barriers is assumed to be much thicker than the InGaN QW, which ensures the evanescence of the envelope wave functions in the GaN barriers for both conduction band and valence band. The potential band lineups are solved self-consistently based on the Poisson's equation [17]. The convergence condition is set such as the tolerance of the eigen energy is less than 0.1%.

IV. Optimization of Staggered InGaN QW for 500 nm

Fig. 2 shows the energy band lineup profiles and the wave functions of the first conduction subband (C1) and the first valence subband (HH1) at zone center for (a) conventional 30-Å $In_{0.25}Ga_{0.75}N$ QW, (b) two-layer staggered 18-Å $In_{0.3}Ga_{0.7}N$/12-Å $In_{0.14}Ga_{0.86}N$ QW and (c) three-layer staggered 6-Å $In_{0.14}Ga_{0.86}N$/18-Å $In_{0.3}Ga_{0.7}N$/6-Å $In_{0.14}Ga_{0.86}N$ QW. The structures are designed such that all three QWs emit at ~500 nm. As shown in Fig. 2(a), a large spatial separation between electron and hole wave functions is observed in the conventional InGaN QW due to the existence of the internal electric field and with the electron–hole wave function overlap ($\Gamma_{\mathrm{e\_hh}}$) of 17.35%. Fig. 2(b) shows the two-layer staggered InGaN QW design employing a step-function like In content for the QW, and the use of these two-layer design leads to the electron wave function being pushed to the center of the QW resulting in enhanced electron–hole wave function overlap ($\Gamma_{\mathrm{e\_hh}}$) of 27.6%. Fig. 2(c) shows three-layer staggered InGaN QW with higher In-content sublayer in the center sandwiched between two sublayers with lower In-content. In the three-layer QW, both the electron and hole wave functions are pushed to the center of the QW resulting in increase in the electron–hole wave function overlap ($\Gamma_{\mathrm{e\_hh}}$) of 31.22%. By optimizing the In contents and thicknesses of the sublayers for both two-layer staggered InGaN QW and three-layer staggered InGaN QW, the electron–hole wave function overlap ($\Gamma_{\mathrm{e\_hh}}$) of the staggered InGaN QW is improved by 1.6–1.8 times.

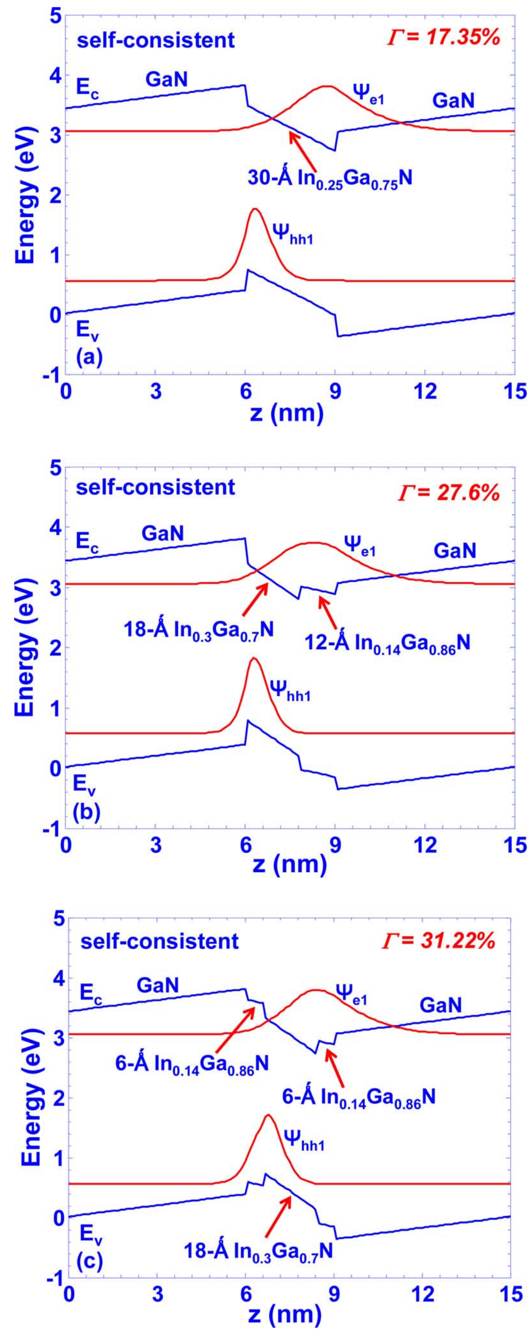

Fig. 2. Energy band lineups of (a) conventional 30-Å $In_{0.25}Ga_{0.75}N$ QW, (b) two-layer staggered 18-Å $In_{0.3}Ga_{0.7}N$/12-Å $In_{0.14}Ga_{0.86}N$ QW and, (c) three-layer staggered 6-Å $In_{0.14}Ga_{0.86}N$/18-Å $In_{0.3}Ga_{0.7}N$/6-Å $In_{0.14}Ga_{0.86}N$ QW. All three QW structures are designed for $\lambda \sim 500$ nm.

Fig. 3 shows the calculated spontaneous emission spectra for conventional InGaN QW (dash-dot line), two-layer staggered InGaN QW (dash line), and three-layer staggered InGaN QW (solid line) at carrier densities (N) of $N = 2$–10×10^{18} cm^{-3} at $T = 300$ K. The spontaneous emission rate is obtained by taking into account all possible transitions between nth conduction

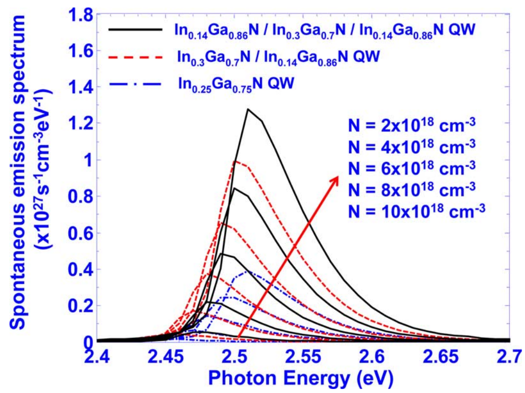

Fig. 3. Spontaneous emission spectra for conventional 30-Å $In_{0.25}Ga_{0.75}N$ QW, two-layer staggered 18-Å $In_{0.3}Ga_{0.7}N$/12-Å $In_{0.14}Ga_{0.86}N$ QW, and three-layer staggered 6-Å $In_{0.14}Ga_{0.86}N$/18-Å $In_{0.3}Ga_{0.7}N$/6-Å $In_{0.14}Ga_{0.86}N$ QW emitting at ~500 nm for increasing carrier density $N = 2–10 \times 10^{18}$ cm^{-3}.

subbands and mth valence subbands as follow

$$r^{\text{spon}}(\hbar\omega) = \frac{2q^2\pi}{n_r c\varepsilon_0 m_0^2 \omega L_\omega} \sum_{\sigma=U,L} \sum_{n,m} \int \frac{k_t dk_t}{2\pi} |(M)_{nm}(k_t)|^2 \times \frac{f_n^{\text{c}}(k_t)\left(1 - f_{\sigma m}^{\text{v}}(k_t)\right)(\gamma/\pi)}{\left(E_{\sigma,nm}^{\text{cv}}(k_t) - \hbar\omega\right)^2 + \gamma^2} \quad (1)$$

where $f_n^{\text{c}}(k_t)$ and $f_{\sigma m}^{\text{v}}(k_t)$ are the Fermi-Dirac distribution functions for the electrons in conduction band and valence band, and k_t is the in-plane wave vector, L_ω is the thickness of the QW, $(M)_{nm}(k_t)$is the momentum matrix element between nth conduction subband and mth valence subband. Due to the asymmetry of the band lineups for the conduction band and valence band, the transitions between states with unequal quantum numbers ($m \neq n$) are nonzero. In this calculation, all possible transitions between the confined states of the conduction bands and valence bands are taken into account.

From Fig. 3, the spontaneous emission spectra for staggered InGaN QWs are significantly enhanced as compared to that of the conventional InGaN QW for each carrier density. For the case of $N = 10 \times 10^{18}$ cm^{-3}, the two-layer staggered InGaN QW shows approximately 2.54 times higher of the peak spontaneous emission spectra (9.96×10^{26} s^{-1} cm^{-3} eV^{-1}) than that of the conventional one (3.9×10^{26} s^{-1} cm^{-3} eV^{-1}). The three-layer staggered InGaN QW (12.8×10^{26} s^{-1} cm^{-3} eV^{-1}) shows 3.26 times higher than that of the conventional InGaN QW. Note that the peaks of the spontaneous emission spectra for both the conventional InGaN QW and staggered InGaN QWs show blue shift as the carrier density increases.

The total spontaneous emission radiative recombination rate per unit volume (s^{-1} cm^{-3}) is obtained by integrating the (1) over the entire frequency range as follow

$$R_{\text{sp}} = \int_0^\infty r^{\text{spon}}(\hbar\omega)\, d(\hbar\omega). \quad (2)$$

Fig. 4(a) illustrates the spontaneous emission radiative recombination rate per unit volume (R_{sp}) for the conventional InGaN QW, the two-layer staggered InGaN QW and the three-layer staggered InGaN QW as a function of the carrier density up to 10×10^{18} cm^{-3}. Fig. 4(b) shows the ratio of the spontaneous emission radiative recombination rate (R_{sp}) for two-layer staggered InGaN QW and conventional InGaN QW as well as the ratio for three-layer staggered InGaN QW and conventional InGaN QW for carrier density $N = 1 \times 10^{18}$ cm^{-3} up to $N = 10 \times 10^{18}$ cm^{-3}. For the two-layer staggered InGaN QW, the enhancement of the spontaneous emission radiative recombination rate (R_{sp}) ranges between 2.6 and 2.8 times at each carrier density as compared to the conventional InGaN QW. The enhancement of the R_{sp} for the three-layer staggered InGaN QW as compared to the conventional InGaN QW ranges between 3.3 and 3.7 times.

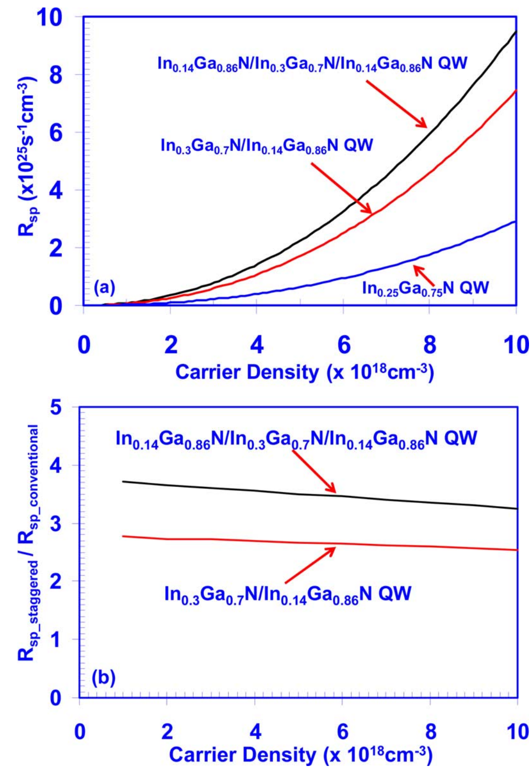

Fig. 4. (a) Spontaneous emission radiative recombination rate (R_{sp}) as a function of carrier density for conventional 30-Å $In_{0.25}Ga_{0.75}N$ QW, two-layer staggered 18-Å $In_{0.3}Ga_{0.7}N$/12-Å $In_{0.14}Ga_{0.86}N$ QW, and three-layer staggered 6-Å $In_{0.14}Ga_{0.86}N$/18-Å $In_{0.3}Ga_{0.7}N$/6-Å $In_{0.14}Ga_{0.86}N$ QW at room temperature. (b) The ratio of spontaneous emission radiative recombination rate for staggered InGaN QW and conventional InGaN QW.

V. Optimization of Staggered InGaN QW for 540 nm

In this section, similar concepts of two-layer and three-layer staggered InGaN QWs are implemented to optimize the electron–hole wave function overlap ($\Gamma_{\text{e\_hh}}$) for InGaN QWs emitting at $\lambda \sim 540$ nm. The optimized QW structures are: 1) conventional 35-Å $In_{0.27}Ga_{0.73}N$ QW; 2) two-layer staggered 21-Å $In_{0.32}Ga_{0.68}N$/14-Å $In_{0.16}Ga_{0.84}N$ QW; and 3) three-layer staggered 7-Å $In_{0.16}Ga_{0.84}N$/21-Å $In_{0.32}Ga_{0.68}N$/7-Å $In_{0.16}Ga_{0.84}N$ QW. All the three structures are designed for similar peak emission wavelengths at $\lambda \sim 540$ nm.

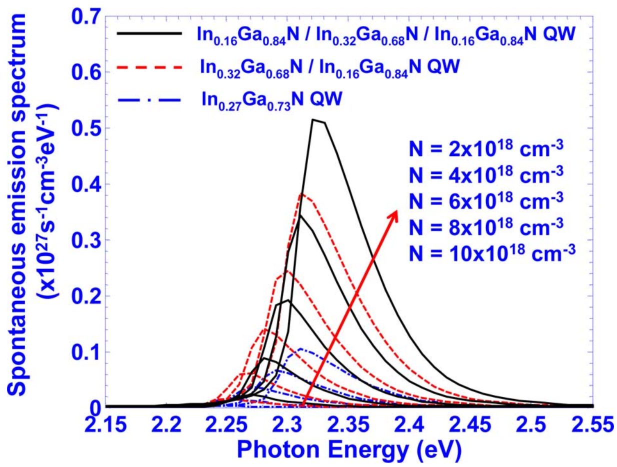

Fig. 5. Spontaneous emission spectra for conventional 35-Å $In_{0.27}Ga_{0.73}N$ QW, two-layer staggered 21-Å $In_{0.32}Ga_{0.68}N$/14-Å $In_{0.16}Ga_{0.84}N$ QW, and three-layer staggered 7-Å $In_{0.16}Ga_{0.84}N$/21-Å $In_{0.32}Ga_{0.68}N$/7-Å $In_{0.16}Ga_{0.84}N$ QW emitting at ~ 540 nm for increasing carrier density $N = 2$–10×10^{18} cm^{-3}.

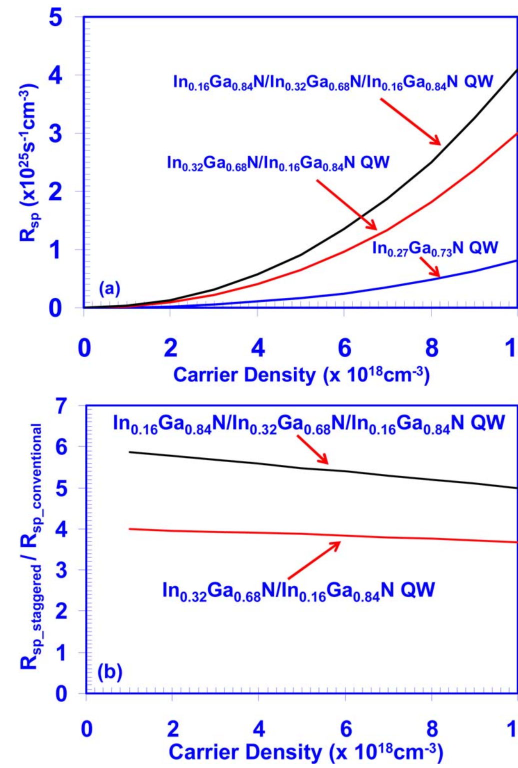

Fig. 6. (a) Spontaneous emission radiative recombination rate (R_{sp}) as a function of carrier density for conventional 35-Å $In_{0.27}Ga_{0.73}N$ QW, two-layer staggered 21-Å $In_{0.32}Ga_{0.68}N$/14-Å $In_{0.16}Ga_{0.84}N$ QW, and three-layer staggered 7-Å $In_{0.16}Ga_{0.84}N$/21-Å $In_{0.32}Ga_{0.68}N$/7-Å $In_{0.16}Ga_{0.84}N$ QW at room temperature. (b) The ratio of spontaneous emission radiative recombination rate for staggered InGaN QW and conventional InGaN QW.

Fig. 5 shows the comparison of the R_{sp} for the conventional InGaN QW, two-layer staggered InGaN QW, and three-layer staggered InGaN QW emitting at $\lambda \sim 540$ nm. The R_{sp} spectra in Fig. 5 show a significant enhancement of the spontaneous emission radiative recombination rate for both two-layer staggered InGaN QW and three-layer staggered InGaN QW. For example, at $N = 10 \times 10^{18}$ cm^{-3}, the two-layer staggered InGaN QW (3.83×10^{26} s^{-1} cm^{-3} eV^{-1}) shows 3.65 times improvement of the peak R_{sp} as compared to that of the conventional InGaN QW (1.05×10^{26} s^{-1} cm^{-3} eV^{-1}), while the three-layer staggered InGaN QW (5.14×10^{26} s^{-1} cm^{-3} eV^{-1}) shows 4.9 times improvement. Note that as the emission wavelength is extended from 500 nm to 540 nm, the absolute values of the R_{sp} become smaller due to the reduced electron–hole wave function overlap ($\Gamma_{\mathrm{e\_hh}}$) from the use of thicker QW and higher In-content InGaN QW.

Fig. 6(a) shows the comparison of the spontaneous emission rate for the conventional two-layer staggered and three-layer staggered InGaN QWs emitting at 540-nm spectral regime. As shown in Fig. 6(b), the ratios of the R_{sp} of the staggered InGaN QWs structures with that of the conventional InGaN QW are compared for QWs active regions emitting in 540-nm spectral regime. As the carrier density increases from 1×10^{18} cm^{-3} to 10×10^{18} cm^{-3}, the ratio of the R_{sp} ratio of the two-layer staggered InGaN QW and conventional InGaN QW is 3.66–4. For the case of three-layer staggered InGaN QW, the ratio improvement of 5–5.86 is observed.

By comparing Figs. 4(b) and 6(b), the R_{sp} improvement for the case of longer emission wavelength ($\lambda \sim 540$ nm) is larger than that of the emission wavelength of $\sim$500 nm. The approach of using the staggered InGaN QW to enhance the electron–hole wave function overlap ($\Gamma_{\mathrm{e_hh}}$) has more advantages for the case of the longer emission wavelength, in particular as the charge separation becomes increasingly significant resulting in low electron–hole wave function overlap ($\Gamma_{\mathrm{e_hh}}$).

VI. Carrier Lifetime and Radiative Efficiency Analysis for Staggered InGaN QWs

A. *Formulation of Carrier Lifetime and Radiative Efficiency*

The external quantum efficiency (η_{external}) of III-Nitride LEDs devices can be expressed as function of current injection efficiency (η_{inj}), radiative efficiency (η_{Rad}), and light extraction efficiency ($\eta_{\mathrm{extraction}}$), as follow [22]:

$$\eta_{\mathrm{external}} = \eta_{\mathrm{inj}} \cdot \eta_{\mathrm{Rad}} \cdot \eta_{\mathrm{extraction}}. \tag{3}$$

Note that the current injection efficiency (η_{inj}) represents fraction of the injected current that recombines in the QW active region [22]. The radiative efficiency (η_{Rad}) represents fraction of recombination current in the QW that recombines radiatively resulting in photon generation, and the light extraction efficiency ($\eta_{\mathrm{extraction}}$) represents fraction of the generated photon in the QW that can be extracted out of the semiconductor cavity into free space.

Here, we will investigate only the radiative efficiency from the implementation of staggered InGaN QWs as active region in III-Nitride LEDs for green emission. However, it is important to note that optimization of both current injection efficiency and light extraction efficiency in InGaN QW LEDs as important factors to optimize the total external quantum efficiency of the III-Nitride LEDs.

The total recombination current density in semiconductor QW active regions can be expressed as follow

$$\eta_{\rm inj} \cdot J = J_{\rm QW} = q \cdot d_{\rm QW} \cdot \left(A \cdot N + R_{\rm sp} + C \cdot N^3\right) \quad (4)$$

where $\eta_{\rm inj}$ is the current injection efficiency, J is the injected current density, and $d_{\rm QW}$ is the thickness of the QW active regions. The $J_{\rm QW}$ represents the total recombination current in the QWs. The parameters A and C represent the monomolecular and Auger recombination rate coefficients, respectively, and the parameter $R_{\rm sp}$ is the radiative recombination rate. The parameter N is the carrier density in the QW active region.

The total carrier recombination rate in the QW active region can be expressed as:

$$R_{\rm total} = A \cdot N + R_{\rm sp} + C \cdot N^3. \quad (5)$$

The radiative recombination rate ($R_{\rm sp}$) can be obtained from (1) and (2), and the results have been discussed in Sections IV and V. Thus the radiative efficiency can be obtained as follow

$$\eta_{\rm Rad} = \frac{R_{\rm sp}}{R_{\rm non\_rad} + R_{\rm sp}} \quad (6)$$

where the $R_{\rm non\_rad}$ consists of both the monomolecular and Auger recombination rate in the QW as follow:

$$R_{\rm non\_rad} = A \cdot N + C \cdot N^3. \quad (7)$$

Due to the negligible value of the Auger coefficient in the InGaN-based wide bandgap material system [23], [24], the non-radiative part only take into account the monomolecular recombination in this analysis. Thus, the radiative efficiency of InGaN QW LEDs can be expressed as:

$$\eta_{\rm Rad} = \frac{R_{\rm sp}}{A \cdot N + R_{\rm sp}}. \quad (8)$$

Further discussion on the impacts of Auger recombination on the radiative efficiency of InGaN QW LEDs will be discussed on Section VII.

The total carrier recombination rate ($R_{\rm total}$) can be expressed as a function of carrier lifetime ($\tau_{\rm total}$) and carrier density in the QW (N) as follow:

$$R_{\rm total} = R_{\rm sp} + R_{\rm non\_rad} = \frac{N}{\tau_{\rm total}}. \quad (9)$$

The total carrier lifetime ($\tau_{\rm total}$) composes of both the radiative lifetime ($\tau_{\rm rad}$) and nonradiative lifetime ($\tau_{\rm non\_rad}$), as follow

$$\frac{1}{\tau_{\rm total}} = \frac{1}{\tau_{\rm rad}} + \frac{1}{\tau_{\rm non\_rad}} \quad (10)$$

where the parameters $1/\tau_{\rm rad}$ and $1/\tau_{\rm non\_rad}$ can be expressed as

$$\frac{1}{\tau_{\rm rad}} = \frac{R_{\rm sp}}{N} \quad (11)$$

$$\frac{1}{\tau_{\rm non\_rad}} = \frac{R_{\rm non\_rad}}{N}. \quad (12)$$

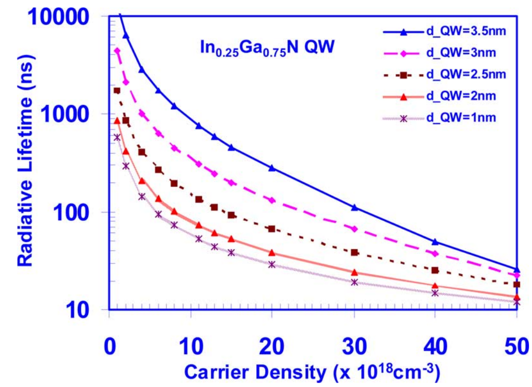

Fig. 7. Radiative lifetime for $In_{0.25}Ga_{0.75}N$ QWs with various QW thickness of 1 nm, 2 nm, 2.5 nm, 3 nm, and 3.5 nm as a function of the carrier density up to 50×10^{18} cm^{-3}.

B. Radiative Recombination and Carrier Lifetime Analysis

In the III-Nitride material system, the existence of the electrostatic field results in the spatial separation of the electrons and holes, which leads to a longer carrier lifetime. Thus, the radiative carrier lifetime ($\tau_{\rm rad}$) in the conventional InGaN QW system depends on the In content and the QW thickness. Fig. 7 shows the radiative carrier lifetime ($\tau_{\rm rad}$) for conventional $In_{0.25}Ga_{0.75}N$ QW with various QW thickness ($d_{\rm QW} = 1$ nm, 2 nm, 2.5 nm, 3 nm, and 3.5 nm) as a function of the carrier density up to 50×10^{18} cm^{-3}. The five different cases exhibit similar trend: the radiative carrier lifetime ($\tau_{\rm rad}$) decreases as the carrier density increases. And the radiative carrier lifetime ($\tau_{\rm rad}$) increases as the QW thickness increases. For example, at $N = 30 \times 10^{18}$ cm^{-3}, $\tau_{\rm rad} = 19.5$ ns ($d_{\rm QW} = 1$ nm, $\lambda \sim 411$ nm), $\tau_{\rm rad} = 24.4$ ns ($d_{\rm QW} = 2$ nm, $\lambda \sim 452$ nm), $\tau_{\rm rad} = 38.6$ ns ($d_{\rm QW} = 2.5$ nm, $\lambda \sim 473$ nm), $\tau_{\rm rad} = 66.2$ ns ($d_{\rm QW} = 3$ nm, $\lambda \sim 500$ nm), $\tau_{\rm rad} = 113$ ns ($d_{\rm QW} = 3.5$ nm, $\lambda \sim 510$ nm). These calculated results are comparable to the results in [5] and [23], calculated for conventional InGaN QW active region.

Fig. 8 compares the radiative lifetime ($\tau_{\rm rad}$) for the conventional InGaN QW, two-layer staggered InGaN QW, and three-layer staggered InGaN QW as a function of the carrier density up to 50×10^{18} cm^{-3} for the QW structures discussed in Section IV [Fig. 8 (a)] and Section V [Fig. 8(b)], respectively. For both cases, the radiative carrier lifetime ($\tau_{\rm rad}$) of the staggered InGaN QWs is reduced due to the improved spontaneous emission radiative recombination rate ($R_{\rm sp}$) as compared to that of the conventional InGaN QW. From Fig. 8(a), the radiative carrier lifetime ($\tau_{\rm rad}$) of the two-layer staggered InGaN QW is reduced by 35%–64% as compared to that of the conventional InGaN QW at different carrier density, while the radiative carrier lifetime ($\tau_{\rm rad}$) of the three-layer staggered InGaN QW is reduced by 40%–73% ($\lambda \sim 500$ nm). From Fig. 8(b), the radiative carrier lifetime ($\tau_{\rm rad}$) of the two-layer staggered InGaN QW is reduced by 39%–75%, and the radiative carrier lifetime ($\tau_{\rm rad}$) of the three-layer staggered InGaN QW is reduce by 41%–83%.

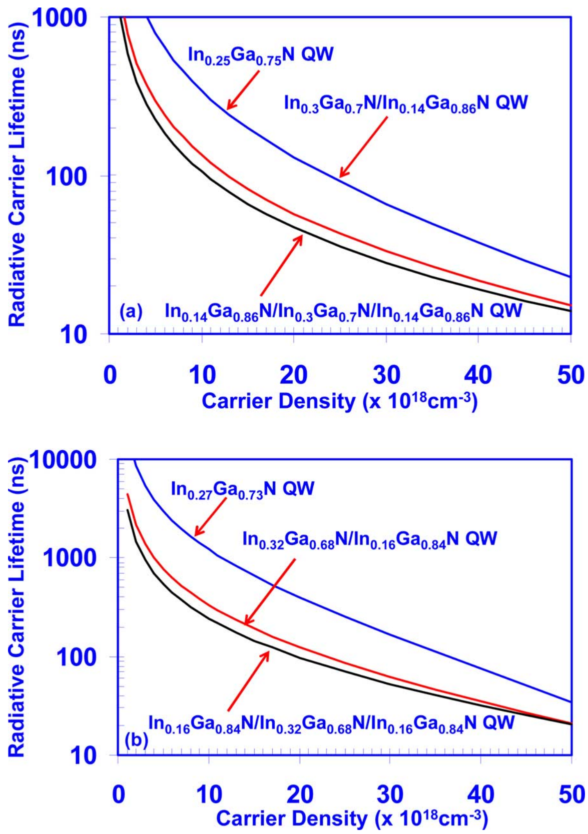

Fig. 8. Radiative lifetime for (a) conventional 30-Å $In_{0.25}Ga_{0.75}N$ QW, two-layer staggered 18-Å $In_{0.3}Ga_{0.7}N$/12-Å $In_{0.14}Ga_{0.86}N$ QW, and three-layer staggered 6-Å $In_{0.14}Ga_{0.86}N$/18-Å $In_{0.3}Ga_{0.7}N$/6-Å $In_{0.14}Ga_{0.86}N$ QW emitting at ∼500 nm as a function of the carrier density up to $50 \times 10^{18}\,cm^{-3}$, (b) conventional 35-Å $In_{0.27}Ga_{0.73}N$ QW, two-layer staggered 21-Å $In_{0.32}Ga_{0.68}N$/14-Å $In_{0.16}Ga_{0.84}N$ QW, and three-layer staggered 7-Å $In_{0.16}Ga_{0.84}N$/21-Å $In_{0.32}Ga_{0.68}N$/7-Å $In_{0.16}Ga_{0.84}N$ QW emitting at ∼540 nm as a function of the carrier density up to $50 \times 10^{18}\,cm^{-3}$.

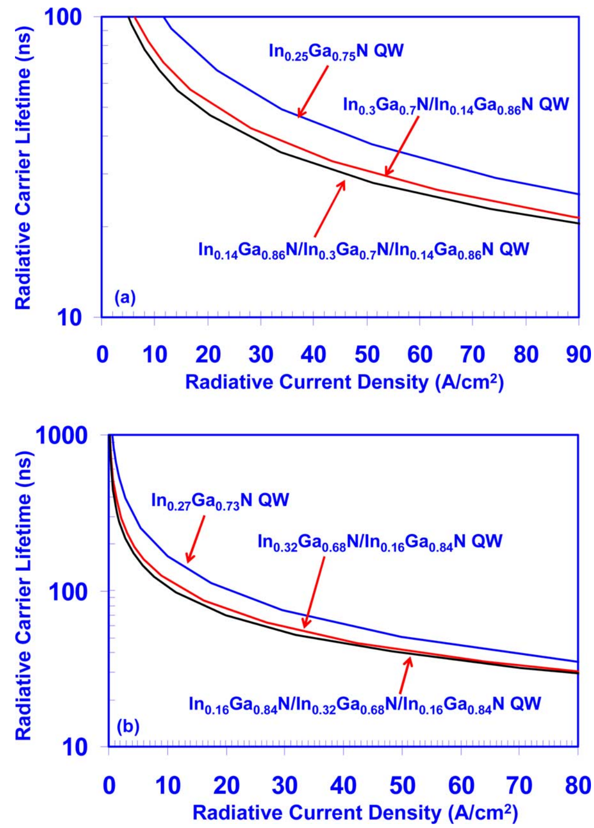

Fig. 9. Radiative lifetimes for (a) conventional 30-Å $In_{0.25}Ga_{0.75}N$ QW, two-layer staggered 18-Å $In_{0.3}Ga_{0.7}N$/12-Å $In_{0.14}Ga_{0.86}N$ QW, and three-layer staggered 6-Å $In_{0.14}Ga_{0.86}N$/18-Å $In_{0.3}Ga_{0.7}N$/6-Å $In_{0.14}Ga_{0.86}N$ QW emitting at ∼500 nm as a function of the radiative current density, (b) conventional 35-Å $In_{0.27}Ga_{0.73}N$ QW, two-layer staggered 21-Å $In_{0.32}Ga_{0.68}N$/14-Å $In_{0.16}Ga_{0.84}N$ QW, and three-layer staggered 7-Å $In_{0.16}Ga_{0.84}N$/21-Å $In_{0.32}Ga_{0.68}N$/7-Å $In_{0.16}Ga_{0.84}N$ QW emitting at ∼540 nm as a function of the radiative current density.

The relation of the radiative current density and radiative recombination rate is related by the following equation:

$$J_{\mathrm{rad}} = q \cdot d_{\mathrm{QW}} \cdot R_{\mathrm{sp}}. \tag{13}$$

To better understand the relationship between the carrier lifetime and the current density, Fig. 9(a) and (b) show the radiative carrier lifetime (τ_{rad}) versus the radiative current density for the conventional, two-layer staggered, and three-layer staggered InGaN QWs emitting at 500 nm [Fig. 9(a)] and 540 nm [Fig. 9(b)]. Fig. 9(a) and (b) show similar trend as those of Fig. 8(a) and (b), which indicate that the radiative carrier lifetimes for staggered InGaN QWs (both two-layer and three-layer staggered InGaN QWs) structures significantly reduces, in comparison to that of the conventional InGaN QW for the radiative current density analyzed up to 90 A/cm^2. Note that the longer radiative lifetimes observed for InGaN QWs emitting in the 500 nm and 540 nm is a result of the lower optical matrix element in these QWs, in comparison to those observed for blue-emitting InGaN QWs active regions.

C. Total Recombination Processes and Radiative Efficiency

The total carrier recombination rate (R_{total}) and carrier lifetime (τ_{total}) can be obtained from (5) and (9), respectively. Note that in the current analysis, we have only taken into account the monomolecular recombination processes. The monomolecular recombination coefficient (A) have been widely reported from the range of $A = 1 \times 10^7$ s^{-1} up to $A = 3 \times 10^8$ s^{-1} [25]–[27], and these discrepancies on the reported values can be attributed to the varying material quality reported by different groups. As our goal is to investigate the limitation presented by relatively high-quality InGaN QW with low dislocation density, we employed the experimentally reported monomolecular recombination coefficient $A = 3 \times 10^7$ s^{-1} similar to the experiment results reported in [25]. Further discussion on the impacts of Auger recombination in InGaN QW will be discussed separately in Section VII.

The total carrier recombination lifetimes as functions of carrier density in the QWs are plotted in Fig. 10(a) and (b) for QWs emitting in the 500 nm and 540 nm, respectively. It is interesting to note that significant reduction in the total carrier lifetimes were observed due to the use of staggered InGaN QWs. The use of three-layer staggered InGaN QW leads to the most

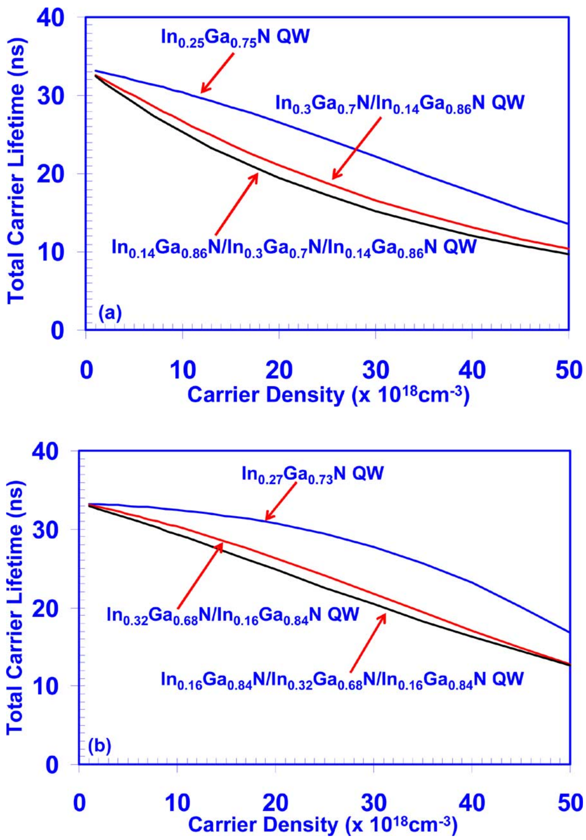

Fig. 10. Total carrier lifetimes for (a) conventional 30-Å $In_{0.25}Ga_{0.75}N$ QW, two-layer staggered 18-Å $In_{0.3}Ga_{0.7}N$/12-Å $In_{0.14}Ga_{0.86}N$ QW, and three-layer staggered 6-Å $In_{0.14}Ga_{0.86}N$/18-Å $In_{0.3}Ga_{0.7}N$/6-Å $In_{0.14}Ga_{0.86}N$ QW emitting at ~500 nm as a function of the carrier density up to 50×10^{18} cm^{-3}, (b) conventional 35-Å $In_{0.27}Ga_{0.73}N$ QW, two-layer staggered 21-Å $In_{0.32}Ga_{0.68}N$/14-Å $In_{0.16}Ga_{0.84}N$ QW, and three-layer staggered 7-Å $In_{0.16}Ga_{0.84}N$/21-Å $In_{0.32}Ga_{0.68}N$/7-Å $In_{0.16}Ga_{0.84}N$ QW emitting at ~540 nm as a function of the carrier density up to 50×10^{18} cm^{-3}.

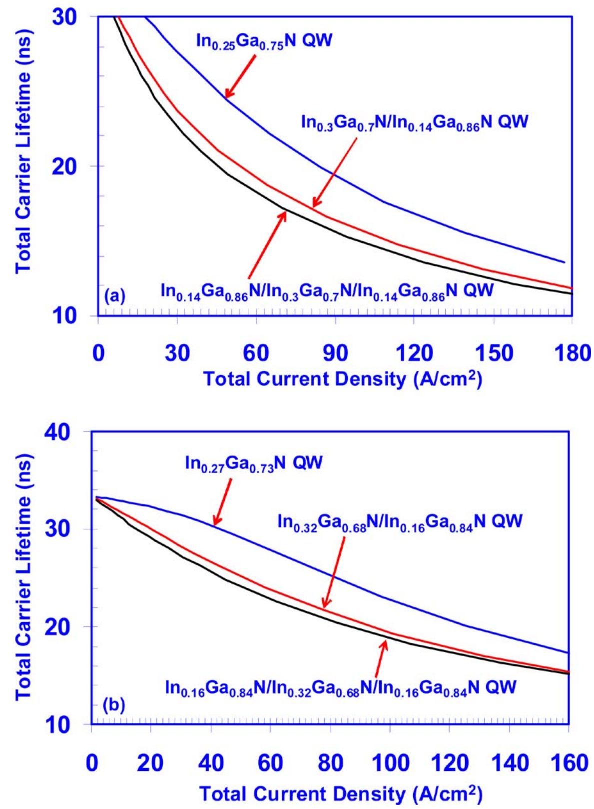

Fig. 11. Total carrier lifetime for (a) conventional 30-Å $In_{0.25}Ga_{0.75}N$ QW, two-layer staggered 18-Å $In_{0.3}Ga_{0.7}N$/12-Å $In_{0.14}Ga_{0.86}N$ QW, and three-layer staggered 6-Å $In_{0.14}Ga_{0.86}N$/18-Å $In_{0.3}Ga_{0.7}N$/6-Å $In_{0.14}Ga_{0.86}N$ QW emitting at ~500 nm as a function of the total current density, (b) conventional 35-Å $In_{0.27}Ga_{0.73}N$ QW, two-layer staggered 21-Å $In_{0.32}Ga_{0.68}N$/14-Å $In_{0.16}Ga_{0.84}N$ QW, and three-layer staggered 7-Å $In_{0.16}Ga_{0.84}N$/21-Å $In_{0.32}Ga_{0.68}N$/7-Å $In_{0.16}Ga_{0.84}N$ QW emitting at ~540 nm as a function of the total current density.

optimized QW structures with lowest carrier lifetimes. Note that all the QWs studied here assumed similar monomolecular recombination coefficient (A). The use of low A value is realistic in particular for high-quality InGaN QW material, and the reported carrier lifetimes here are comparable with the total carrier lifetimes reported from experiments [27], [28].

Fig. 11(a) and (b) show the total carrier lifetime versus the total current density for conventional, two-layer staggered, and three-layer staggered InGaN QWs emitting at 500 nm [Fig. 11(a)] and 540 nm [Fig. 11(b)]. Fig. 11(a) and (b) indicate that the total carrier lifetime decrease for both two-layer and three-layer staggered InGaN QWs as compared to that of the conventional InGaN QW for both structures emitting at 500 nm and 540 nm.

Based on (8), the radiative efficiency (η_{Rad}) as a function of carrier density (N) in QW is calculated for the conventional InGaN QW, two-layer staggered InGaN QW and three-layer staggered InGaN QW for the structures discussed in Sections IV and V as shown in Fig. 12(a) and (b). The carrier density in the QW was calculated up to 5×10^{19} cm^{-3}. Note that the radiative efficiency (η_{Rad}) increases as the carrier density increases, due to the stronger carrier dependency of the radiative recombination rate (R_{sp}). For the QW structures with the emission wavelength of 500 nm [Fig. 12(a)], the radiative efficiency (η_{Rad}) is enhanced by 1.52–2.74 times and 1.64–3.64 times for the two-layer staggered InGaN QW and three-layer staggered InGaN QW as compared to that of the conventional InGaN QW. Fig. 12(b) shows that the radiative efficiency (η_{Rad}) is increased by 1.24–3.97 times and 1.26–5.81 times for the two-layer staggered InGaN QW and three-layer staggered InGaN QW at the emission wavelength of 540 nm. In the low carrier density regime, the conventional InGaN QWs exhibited relatively low radiative efficiency, while both the staggered InGaN QW designs exhibited significantly higher radiative efficiency. Only at very high carrier density level, the radiative recombination rate in the conventional InGaN QW design increases. However, it is important to note that high carrier density operation may not be favorable for optimized InGaN QW LED device operation; in particular thermionic carrier leakage may limit the current injection efficiency in QW LEDs or laser devices [22].

The reduction of the carrier lifetimes in staggered QW designs leads to the enhancement of the radiative efficiency. Fig. 13(a) and (b) show the radiative efficiency versus the total current density for conventional, two-layer staggered, and three-layer staggered InGaN QWs emitting at 500 nm [Fig. 13(a)] and

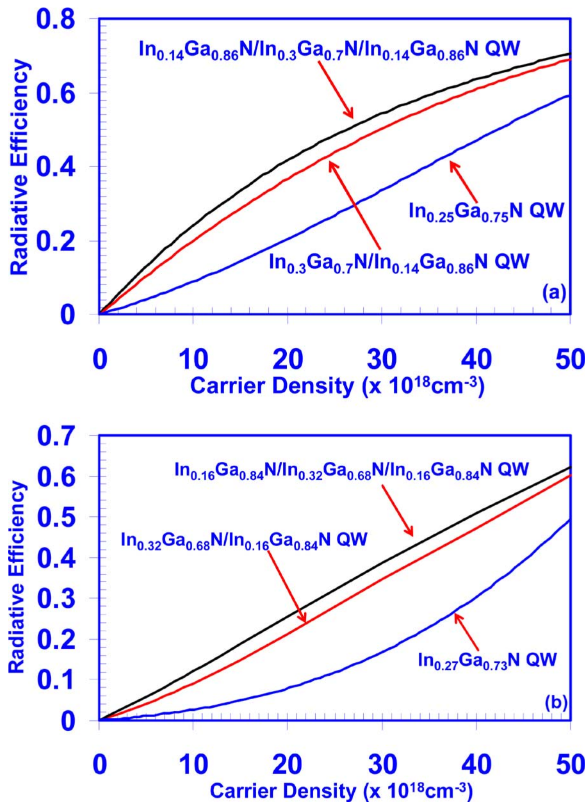

Fig. 12. Radiative efficiency for (a) conventional 30-Å $In_{0.25}Ga_{0.75}N$ QW, two-layer staggered 18-Å $In_{0.3}Ga_{0.7}N$/12-Å $In_{0.14}Ga_{0.86}N$ QW, and three-layer staggered 6-Å $In_{0.14}Ga_{0.86}N$/18-Å $In_{0.3}Ga_{0.7}N$/6-Å $In_{0.14}Ga_{0.86}N$ QW emitting at ~500 nm as a function of the carrier density up to 50×10^{18} cm^{-3}, (b) conventional 35-Å $In_{0.27}Ga_{0.73}N$ QW, two-layer staggered 21-Å $In_{0.32}Ga_{0.68}N$/14-Å $In_{0.16}Ga_{0.84}N$ QW, and three-layer staggered 7-Å $In_{0.16}Ga_{0.84}N$/21-Å $In_{0.32}Ga_{0.68}N$/7-Å $In_{0.16}Ga_{0.84}N$ QW emitting at ~540 nm as a function of the carrier density up to 50×10^{18} cm^{-3}.

540 nm [Fig. 13(b)]. Fig. 13(a) and (b) show similar trend as Fig. 12(a) and (b).

By utilizing both of the two-layer and three-layer staggered InGaN QW structures, the electron–hole wave function overlap ($\Gamma_{\mathrm{e\_hh}}$) is greatly enhanced especially when one extends the wavelength to green and longer. The improved electron–hole wave function overlap ($\Gamma_{\mathrm{e\_hh}}$) leads to the enhancement of the spontaneous emission radiative recombination rate (R_{sp}) for the staggered InGaN QWs, which results in the reduced radiative carrier lifetime (τ_{rad}) and improved radiative efficiency (η_{Rad}).

Note that the radiative efficiency presented in both Figs. 12 and 13 did not take into account the contribution of current injection efficiency in the InGaN QW LEDs. It is important to note that the internal efficiency in the III-Nitride LEDs depends on both the contribution from the current injection efficiency and radiative efficiency of InGaN QW active region. The discussion of the current injection efficiency for InGaN QW LEDs is beyond the scope of this paper. The current injection efficiency of QW LEDs and lasers depends strongly on the interplay of carrier capture and thermionic emission of carriers in QW-barrier heterostructures, carrier transports, and carrier recombinations in QW and barrier regions [22].

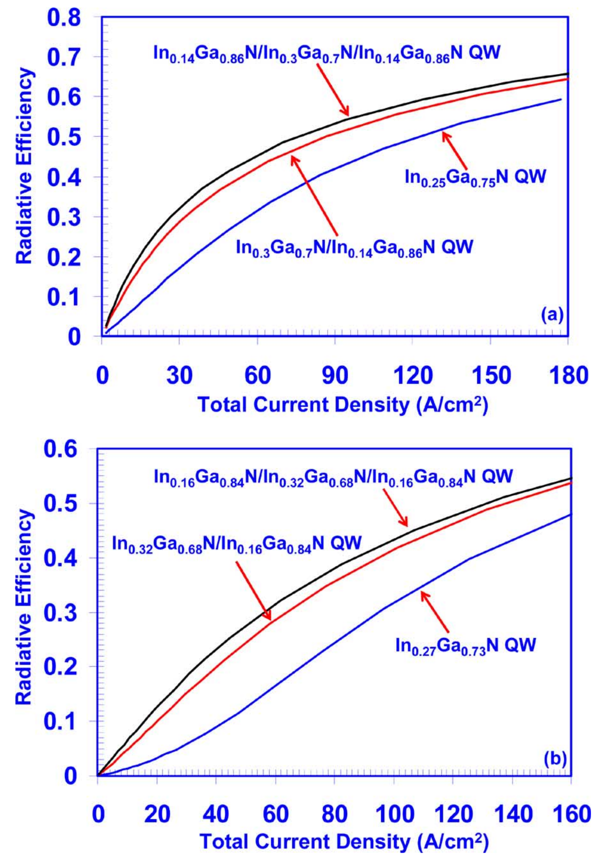

Fig. 13. Radiative efficiency for (a) conventional 30-Å $In_{0.25}Ga_{0.75}N$ QW, two-layer staggered 18-Å $In_{0.3}Ga_{0.7}N$/12-Å $In_{0.14}Ga_{0.86}N$ QW, and three-layer staggered 6-Å $In_{0.14}Ga_{0.86}N$/18-Å $In_{0.3}Ga_{0.7}N$/6-Å $In_{0.14}Ga_{0.86}N$ QW emitting at ~500 nm as a function of the total current density, (b) Conventional 35-Å $In_{0.27}Ga_{0.73}N$ QW, two-layer staggered 21-Å $In_{0.32}Ga_{0.68}N$/14-Å $In_{0.16}Ga_{0.84}N$ QW, and three-layer staggered 7-Å $In_{0.16}Ga_{0.84}N$/21-Å $In_{0.32}Ga_{0.68}N$/7-Å $In_{0.16}Ga_{0.84}N$ QW emitting at ~540 nm as a function of the total current density.

VII. Impacts of Auger Recombination on Radiative Efficiency of InGaN QW LEDs

The Auger recombination rate in wide bandgap III-Nitride semiconductor is predicted to be significantly lower, in comparison to that of monomolecular and radiative recombination rates. Recent theoretical studies predicted Auger recombination coefficients in the range of $C = 3.5 \times 10^{-34}$ cm^6/s [23] up to $C = 0.9$–1×10^{-32} cm^6/s [24]. However, it is important to note that recent experimental studies have indicated the possibility that the Auger recombination coefficient in thick InGaN/GaN double heterostructure active regions ($d_{\mathrm{Active}} =$ 10–77 nm) is in the range of $C = 1.4 \times 10^{-30}$ cm^6/s up to $C = 2 \times 10^{-30}$ cm^6/s [25]. Further studies are still required to clarify and confirm the Auger coefficients (C_{Auger}) for InGaN/GaN QW system, due to the large discrepancies from the reported Auger coefficients in the literatures [23]–[25].

In the radiative efficiency studies presented in Section VI, we specifically did not take into account Auger processes in the analysis. However, in this section, we will present the radiative efficiency analysis of the staggered InGaN QW by taking into

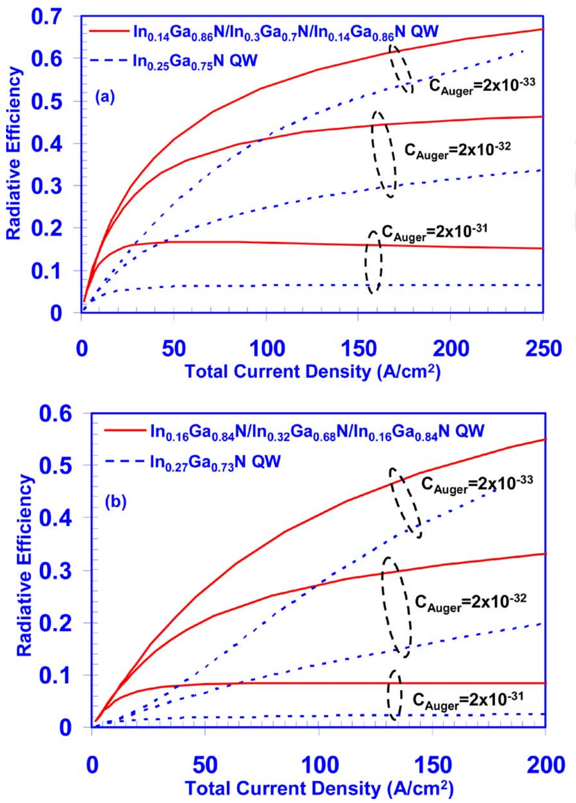

Fig. 14. Radiative efficiency for (a) conventional 30-Å $In_{0.25}Ga_{0.75}N$ QW and three-layer staggered 6-Å $In_{0.14}Ga_{0.86}N$/18-Å $In_{0.3}Ga_{0.7}N$/6-Å $In_{0.14}Ga_{0.86}N$ QW emitting at ∼500 nm as a function of the total current density; (b) conventional 35-Å $In_{0.27}Ga_{0.73}N$ QW, and three-layer staggered 7-Å $In_{0.16}Ga_{0.84}N$/21-Å $In_{0.32}Ga_{0.68}N$/7-Å $In_{0.16}Ga_{0.84}N$ QW emitting at ∼540 nm as a function of total current density. The analyses take into account Auger coefficient from $C = 2 \times 10^{-33}$ cm^6/s (lower limit) up to $C = 2 \times 10^{-31}$ cm^6/s (upper limit).

account both the upper limit and lower limit of the reported Auger coefficients.

Fig. 14(a) [and Fig. 14(b)] shows the radiative efficiency of the 500 nm (and 540 nm) emitting InGaN QW active regions for various design by taking into account $C = 2 \times 10^{-33}$ cm^6/s (lower limit) up to $C = 2 \times 10^{-31}$ cm^6/s (upper limit). As the analysis presented in Fig. 14(a) and (b) are intended to illustrate the trends in the radiative efficiency characteristics of staggered InGaN QWs by taking into account the Auger recombination process, we provide the comparison studies for the optimized three-layer staggered InGaN QW and conventional InGaN QW. The inclusion of the lower limit Auger coefficient modifies the radiative efficiency relation very slightly, and the radiative efficiency relation appears to be relatively similar to that computed in Fig. 13(a) and (b). However, for the case of upper limit Auger coefficient, the significantly larger Auger recombination rate results in relatively low radiative efficiency at high current injection level for both 500 nm and 540 nm emitting InGaN QWs. The use of staggered InGaN QW results in improvement in radiative efficiency for all Auger coefficients is considered here.

Our analysis indicated that the use of staggered InGaN QW active regions with enhanced radiative recombination rate is significantly more important, in the event that Auger recombination coefficient is large in InGaN QW. The Auger process follows $\sim N^3$ relation, thus the nonradiative processes will be dominant as the carrier density in the QW increases.

VIII. Summary

In summary, two-layer and three-layer staggered InGaN QW active regions were investigated for LEDs at 500- to 540-nm spectral range. Comprehensive design studies were carried out by employing self-consistent 6-band $k{\cdot}p$ band structure model, taking into consideration valence band mixing, strain effect, spontaneous and piezoelectric polarization, and carrier screening effect.

From our studies, the radiative recombination rate and radiative efficiency of staggered InGaN QWs are expected to be significantly enhanced, in comparison to those of conventional InGaN QW. The increase in radiative recombination rate and radiative efficiency obtained in staggered InGaN QWs active region is a result of the enhanced electron–hole wave function overlap in these QW structures. The use of three-layer staggered InGaN QW is also expected to enable design with improved overlap in comparison to that of two-layer staggered InGaN QW. The use of staggered InGaN QW structures with enhanced radiative recombination rate is important for improving radiative efficiency of green LED devices. Although the optimization studies focused on optimization of LED active region, the staggered InGaN QW active region has the potential for achieving high optical gain for laser applications.

References

[1] S. Nakamura, M. Senoh, N. Iwasa, S. Nagahama, T. Yamada, and T. Mukai, "Superbright green InGaN single-quantum-well-structure light-emitting diodes," *Jpn. J. Appl. Phys.*, vol. 34, pp. L1332–L1335, Oct. 1995.

[2] J. Zhang, J. Yang, G. Simin, M. Shatalov, M. A. Khan, M. S. Shur, and R. Gaska, "Enhanced luminescence in InGaN multiple quantum wells with quaternary AlInGaN barriers," *Appl. Phys. Lett.*, vol. 77, pp. 2668–2670, Oct. 2000.

[3] X. Guo, Y. L. Li, and E. F. Schubert, "Efficiency of GaN/InGaN light-emitting diodes with interdigitated mesa geometry," *Appl. Phys. Lett.*, vol. 79, pp. 1936–1938, Sep. 2001.

[4] B. Witzigmann, V. Laino, M. Luisier, U. T. Schwarz, G. Feicht, W. Wegscheider, K. Engl, M. Furitsch, A. Leber, A. Lell, and V. Härle, "Microscopic analysis of optical gain in InGaN/GaN quantum wells," *Appl. Phys. Lett.*, vol. 88, Art. 021104, Jan. 2006.

[5] I. H. Brown, P. Blood, P. M. Smowton, J. D. Thomson, S. M. Olaizola, A. M. Fox, P. J. Parbrook, and W. W. Chow, "Time evolution of the screening of piezoelectric fields in InGaN quantum wells," *IEEE J. Quantum Electron.*, vol. 42, no. 12, pp. 1202–1208, Dec. 2006.

[6] R. M. Farrell, D. F. Feezell, M. C. Schmidt, D. A. Haeger, K. M. Kelchner, K. Iso, H. Yamada, M. Saito, K. Fujito, D. A. Cohen, J. S. Speck, S. P. DenBaars, and S. Nakamura, "Continuous-wave operation of AlGaN-cladding-free nonpolar m-plane InGaN/GaN laser diodes," *Jpn. J. Appl. Phys.*, vol. 46, pp. L761–L763, Aug. 2007.

[7] J. Park and Y. Kawakami, "Photoluminescence property of InGaN single quantum well with embedded AlGaN δ layer," *Appl. Phys. Lett.*, vol. 88, Art. 202107, May 2006.

[8] S. H. Park, J. Park, and E. Yoon, "Optical gain in InGaN/GaN quantum well structures with embedded AlGaN delta layer," *Appl. Phys. Lett.*, vol. 90, Art. 023508, Jan. 2007.

[9] R. A. Arif, Y. K. Ee, and N. Tansu, "Polarization engineering via staggered InGaN quantum wells for radiative efficiency enhancement of light emitting diodes emitting," *Appl. Phys. Lett.*, vol. 91, no. 9, Art. 091110, Aug. 2007.

[10] R. A. Arif, H. Zhao, Y. K. Ee, and N. Tansu, "Spontaneous emission and characteristics of staggered InGaN quantum-well light-emitting diodes," *IEEE J. Quantum Electron.*, vol. 44, no. 6, pp. 573–580, Jun. 2008.

[11] R. A. Arif, H. Zhao, and N. Tansu, "Type-II InGaN-GaNAs quantum wells active regions for lasers applications," *Appl. Phys. Lett.*, vol. 92, no. 1, Art. 011104, Jan. 2008.

[12] H. Zhao, R. A. Arif, and N. Tansu, "Self consistent analysis of Type-II 'W' InGaN-GaNAs quantum well lasers," *J. Appl. Phys.*, vol. 104, no. 5, Art. 043104, Sep. 2008.

[13] H. Zhao, R. A. Arif, Y. K. Ee, and N. Tansu, "Optical gain analysis of strain-compensated InGaN-AlGaN quantum well active regions for lasers emitting at 420–500 nm," *Opt. Quantum Electron.*, vol. 40, no. 5–6, pp. 301–306, Apr. 2008.

[14] H. Zhao, R. A. Arif, Y. K. Ee, and N. Tansu, "Self-consistent analysis of strain-compensated InGaN–AlGaN quantum wells for lasers and light-emitting diodes," *IEEE J. Quantum Electron.*, vol. 45, no. 1, pp. 66–78, Jan. 2009.

[15] S. L. Chuang and C. S. Chang, "A band-structure model of strained quantum-well wurtzite semiconductors," *Semicond. Sci. Technol.*, vol. 12, pp. 252–263, 1997.

[16] S. L. Chuang and C. S. Chang, "$\boldsymbol{k}\bullet\boldsymbol{p}$ method for strained wurtzite semiconductors," *Phys. Rev. B*, vol. 54, pp. 2491–2504, Jul. 1996.

[17] S. L. Chuang, *Physics of Optoelectronics Devices*. New York: Wiley, 1995, ch. 4 and 9.

[18] I. Vurgaftman and J. R. Meyer, *Chapter 2 in Nitride Semiconductor Devices*. New York: Wiley, 2007.

[19] I. Vurgaftman and J. R. Meyer, "Band parameters for nitrogen-containing semiconductors," *J. Appl. Phys.*, vol. 94, pp. 3675–3696, Sep. 2003.

[20] C. G. Van de Walle and J. Neugebauer, "Small valence-band offsets at GaN/InGaN heterojunctions," *Appl. Phys. Lett.*, vol. 70, pp. 2577–2579, 1997.

[21] S. L. Chuang, "Optical gain of strained wurtzite GaN quantum-well lasers," *IEEE J. Quantum Electron.*, vol. 32, no. 10, pp. 1791–1800, Oct. 1996.

[22] N. Tansu and L. J. Mawst, "Current injection efficiency of 1300-nm InGaAsN quantum-well lasers," *J. Appl. Phys.*, vol. 97, no. 5, Art. 054502, Mar. 2005.

[23] J. Hader, J. V. Moloney, A. Thranhardt, and S. W. Koch, "Interband transitions in InGaN quantum wells," in *Nitride Semiconductor Devices*, J. Piprek, Ed. Weinheim, Germany: Wiley-VCH, 2007, ch. 7, p. 164.

[24] J. Hader, J. V. Moloney, B. Pasenow, S. W. Koch, M. Sabathil, N. Linder, and S. Lutgen, "On the importance of radiative and Auger losses in GaN-based quantum wells," *Appl. Phys. Lett.*, vol. 92, Art. 261103, Jul. 2008.

[25] Y. C. Shen, G. O. Mueller, S. Watanabe, N. F. Gardner, A. Munkholm, and M. R. Krames, "Auger recombination in InGaN measured by photoluminescence," *Appl. Phys. Lett.*, vol. 91, Art. 141101, Oct. 2007.

[26] M. F. Schubert, S. Chhajed, J. K. Kim, E. F. Schubert, D. D. Koleske, M. H. Crawford, S. R. Lee, A. J. Fischer, G. Thaler, and M. A. Banas, "Effect of dislocation density on efficiency droop in GaInN/GaN light-emitting diodes," *Appl. Phys. Lett.*, vol. 91, Art. 1231114, Dec. 2007.

[27] J. K. Son, S. N. Lee, H. S. Paek, T. Sakong, K. H. Ha, O. H. Nam, and Y. Park, "Radiative and non-radiative transitions in blue quantum wells embedded in AlInGaN-based laser diodes," *Phys. Stat. Sol. (c)*, vol. 4, no. 7, pp. 2780–2783, May 2007.

[28] U. T. Schwarza, H. Braun, K. Kojima, Y. Kawakami, S. Nagahama, and T. Mukai, "Interplay of built-in potential and piezoelectric field on carrier recombination in green light emitting InGaN quantum wells," *Appl. Phys. Lett.*, vol. 91, Art. 123503, Sep. 2007.

Hongping Zhao received the Bachelor's degree in physics from Nanjing Normal University, Nanjing, China, and the Master's degree in electrical engineering from Southeast University, Nanjing, in 2003 and 2005, respectively. Since January 2007, she has been working toward the Ph.D. degree at the Electrical and Computer Engineering Department, Lehigh University, Bethlehem, PA.

She has authored or coauthored more than 40 refereed journal and conference publications. Her research areas cover device physics, epitaxial growth, and fabrication of semiconductor optoelectronics devices based on semiconductor nanostructures. Her current research interests include fundamental studies and approaches to improve gain and spontaneous emission of visible gain media based on III-Nitride semiconductors for high-performance lasers and MOCVD epitaxy of InN material for quantum dots and solar cell applications. She is also the recipient of the 2008 SPIE Educational Scholarship in optical science and engineering.

Ronald A. Arif received the Bachelor's degree from Nanyang Technological University, Singapore, in 2002, and the Master's and Ph.D. degrees from Lehigh University, Bethlehem, PA, in 2005 and 2008, respectively.

From 2002 to 2003, he had been a Process Engineer with Agilent Technologies, Singapore. Currently, he is with the Department of Electrical and Computer Engineering, Center for Optical Technologies, Lehigh University, Bethlehem, PA, and is also a member of Technical Staff at EpiWorks, Inc., Champaign, IL. His recent research interests include fundamental studies and novel approaches to improve radiative efficiency of visible gain media based on III-Nitride semiconductor nanostructures for high-efficiency LEDs and lasers, in particular for solid-state lighting. He has also authored or coauthored more than 45 refereed journal and conference publications.

Dr. Arif was also a recipient of Sherman Fairchild Fellowship on Solid State Studies at Lehigh.

Nelson Tansu (S'99–M'02) was born on October 1977. He received the B.S. degree in applied mathematics, electrical engineering, and physics (with highest distinction) and the Ph.D. degree in electrical engineering from the University of Wisconsin-Madison, Madison, WI, in 1998 and 2003, respectively.

From July 2003 till April 2009, he was an Assistant Professor and Peter C. Rossin Assistant Professor (Term Chair 2007–2009) in the Department of Electrical and Computer Engineering (ECE) and the Center for Optical Technologies (COT), Lehigh University Beginning May 2009 (till present), he has been appointed as an Associate Professor (with tenure) of Electrical and Computer Engineering, Lehigh University. He has authored or coauthored more than 160 refereed international journal and conference publications, and he also holds several US patents. He had served several times as a panel member for US National Science Foundation, US Department of Defense, and other agencies in US and abroad. He has also given numerous lectures, seminars, and invited talks (total > 35) in universities, research institutions, and conferences in USA, Canada, Europe, and Asia. He serves as the Primary Guest Editor of the IEEE JOURNAL OF SELECTED TOPICS IN QUANTUM ELECTRONICS SPECIAL ISSUE ON SOLID STATE LIGHTING in 2008–2009, and he also serves as an Associate Editor for IEEE PHOTONICS JOURNAL (2009-present) and as Assistant/Associate Editor for *Nanoscale Research Letters* (2007-present). He was also an invited General Participant at the 2008 National Academy of Engineering (NAE)'s U.S. Frontiers of Engineering (FOE) Symposium, and he also serves as the Organizing Committee for the 2009 NAE's U.S. Frontiers of Engineering Symposium. His current research interests include the theoretical and experimental aspects of the physics of semiconductor optoelectronics materials and devices, the physics of low-dimensional semiconductor (nanostructure), and MOCVD and device fabrications of III-Nitride and III-V-Nitride semiconductor optoelectronics devices on GaAs, InP, and GaN substrates. His teaching interests are in the areas of optoelectronics and photonics, semiconductor physics, applied quantum mechanics, and engineering electromagnetism.

Dr. Tansu is a recipient of the 2008 Libsch Early Career Research Award at Lehigh University. He was a recipient of the Bohn Scholarship, the WARF Graduate University Fellowship, the Vilas Graduate University Fellowship, and the Graduate Dissertator Travel Funding Award, the 2003 Harold A. Peterson ECE Best Research Award (1st Prize) at the University of Wisconsin-Madison.